

***R*-matrix Floquet description of multiphoton ionization of Li**

C.-T. Chen and F. Robicheaux

Department of Physics, Auburn University, Auburn, Alabama 36849-5311

(Received 15 February 1996)

We present mixed gauge *R*-matrix Floquet calculations of multiphoton ionization of Li within a single active electron local model potential. The laser frequency ranges from 15 000 to 15 800 cm⁻¹, and at least three photons are needed to ionize the electron in the 2*s* ground state. We found that the measured ionization rate as a function of photon frequency results from ionization processes in different intensity regions of the laser. The experimental angular distribution of the ejected electrons can be explained using the high intensity portion of the laser for both the lowest ionization channel and the first above-threshold ionization channel. The calculated and experimental angular distributions agree well with each other and demonstrate the success of the *R*-matrix approach to the multiphoton ionization processes. [S1050-2947(96)05810-6]

PACS number(s): 32.80.Rm, 32.80.Wr, 32.80.Fb

I. INTRODUCTION

There have been several theoretical methods introduced to describe multiphoton processes in atoms [1–11]. In particular, the Floquet approximation has proved to be successful for most experimental conditions where strong lasers interact with atoms or ions. There are several assumptions in the Floquet approximation. The typical duration of a modern short pulse laser is of the order of a picosecond. Though it is short by its standard, this is long compared to the typical time of transitions between atomic states at the peak of the laser pulse. The laser can thus be considered to be turned on slowly, and the atomic states evolve adiabatically to the Floquet states. The Floquet state is a linear combination of field-free atomic states which are coupled by the laser field; the coupling between the field-free atomic states may be strong or weak depending on the laser frequency and intensity.

Recent experiments [12] measuring the multiphoton ionization of Li in the vicinity of the 3*d*, 4*s*, and 4*d* resonant states demonstrated the success of the Floquet description. With the laser frequency range from 15 000 to 15 800 cm⁻¹, the 2*s* ground state coupled strongly to the 2*p* and the 3*d* states by one and two photons, respectively. Absorbing three photons puts the electron into the continuum. In the simplest model, one may assume that only the ground state, the 2*p* state, and the 3*d* state are important to the ionization process, and neglect all other states. This 3 × 3 Floquet model [12] explains many aspects of the ionization spectrum in the experiment. The experimental measurements include the three-photon ionization spectrum as a function of laser frequency, the energy shift of the ground state at several frequencies, and the angular distributions of the photoelectrons in the three- and four-photon ionization peaks with various frequencies and intensities. The major features of the ionization rate spectrum can be explained by the three-state Floquet calculation. The angular distribution of the ejected electrons was measured for electrons absorbing three photons and those absorbing four photons. These distributions were fit to low-order Legendre polynomials, but no *ab initio* calculations were performed.

In this paper, we present a mixed gauge *R*-matrix calcu-

lation on this system. The basic idea of a mixed gauge transformation was first discussed in Ref. [13]. The theoretical method in this calculation has been described elsewhere [14], and applied to related problems. Dörr *et al.* [8] used a similar method to obtain multiphoton decay rates in H. Our method utilizes a generalized gauge transformation that gradually incorporates part of the interaction between the electron and the laser field into the wave function. The *R*-matrix method and multichannel quantum defect theory are employed to obtain the scattering information. Particularly, the ionization information is extracted from the delay-time matrix [16] which can be obtained from the scattering matrix. A major extension of the method in this calculation is its application to the angular distribution of the photoelectrons. We obtain excellent agreement with all experimental results.

II. THEORETICAL METHODS

In the mixed gauge formulation, the gauge transformation approaches the length gauge at small distance, the velocity gauge at intermediate distances, and acceleration at large distances. The change from one gauge to the next is accomplished smoothly over a range of distances. The Hamiltonian of the mixed gauge approach is more complicated than it is in a pure gauge. In practice, we omit the transformation to the length gauge at small distances to simplify the evaluation of the Hamiltonian matrix.

We approximate the interaction between the 2*s* electron and the core state by a model potential. The potential is parametrized to obtain a good agreement with the neutral Li spectrum [17]. In atomic units (a.u.), we assume the potential has the following form:

$$V(r) = -\frac{1}{r} - \frac{2}{r} e^{-\alpha_1 r} - \alpha_2 e^{-\alpha_3 r} - \frac{\alpha_d}{2r^4} [1 - e^{-(r/r_c)^3}]^2, \quad (1)$$

where $\alpha_d = 0.189$ [18] is the dipole polarizability, and α_1 , α_2 , α_3 , and r_c are free parameters. The radius of the *R*-matrix boundary in the calculation is set to 31 a.u. This ensures that the energies of the low-lying states are close to the spectroscopic values. We list the parameters used in the cal-

TABLE I. Parameters of the model potential in Eq. (1).

	$l=0$	$l \geq 1$
α_1	2.8917	2.8964
α_2	0.9476	3.2052
α_3	1.9664	4.7130
r_c	1.0	1.0

calculation in Table I, and the energy levels of the orbitals that are contained inside the R -matrix volume in Table II. These levels agree with the compilation [17] within 1 cm^{-1} , except for the $3p$ orbital which has a 8-cm^{-1} error in energy. The error in the $3p$ state energy will not cause problems because it is far from resonances with $2s+1$ photon or $2s+3$ photons. The $1s$ state of the model potential is unphysical, and we do not include it in our calculation.

In the multiphoton ionization processes, a channel is identified by a set of quantum numbers associated with it. These quantum numbers are the angular momentum quantum number l , magnetic quantum number m , and the number of photons absorbed by the electron N . The fact that the electron may absorb an arbitrary number of photons increases the total number of channels to be included in the calculation. This number of channels is, however, reduced by the fact that the magnetic quantum number m does not change before and after the interaction as a result of the linear polarization of the laser. Specifically, the ground state of Li is $2s$, and $m=0$ in all the channels. Since the $3d$ orbital is well contained in the R -matrix volume, the two-photon channels ($2s+2\hbar\omega$ is near $3d$ with $\hbar\omega$ the photon energy) are treated as strongly closed in the calculation near the $3d$ resonance. On the other hand, the $4s$ and $4d$ states are not completely contained inside the R -matrix boundary, and the two-photon processes are treated as weakly closed around the $4s$ and $4d$ resonances (the two-photon channel is strongly closed for frequencies less than $16\,000 \text{ cm}^{-1}$, and weakly closed for frequencies greater than $17\,000 \text{ cm}^{-1}$). They are closed at a later stage to obtain the physical scattering matrix.

The ionization information is extracted by using the delay-time matrix [16]

$$Q(E) = -i \frac{dS(E)}{dE} S^\dagger(E), \quad (2)$$

TABLE II. Energy levels of Li for several low-lying configurations. The energies given are in cm^{-1} , and are below-threshold. In the experiment, if the fine structure of a given configuration can be resolved, the level of the state with lower total angular momentum J is chosen.

Configuration	Energy below-threshold (cm^{-1})	
	Present	Experiment
$2s$	43 487.0	43 487.19
$2p$	28 584.4	28 583.53
$3s$	16 280.0	16 281.07
$3p$	12 554.0	12 561.81
$3d$	12 202.8	12 204.11

^aReference [17].

where S is the scattering matrix. The largest eigenvalue of Q , $q_{\max}(E)$, is a function of energy and can be identified as the decay time of a resonance state. Its energy profile is Lorentzian,

$$q_{\max}(E) = \frac{\Gamma}{(E - E_r)^2 + (\Gamma/2)^2}, \quad (3)$$

where E_r is the resonance energy and the width Γ is the ionization rate of the resonance state.

To obtain the angular distribution of the ejected electrons, we need to construct the wave function describing the outgoing electrons. There are different approaches to obtain the angular distribution function (e.g., Dörr *et al.* [8] and Rottke *et al.* [15]). Surprisingly, in the delay-time formulation, the information needed to obtain the wave function of the ejected electrons in the open channels can be obtained from Q . The eigenvector of the delay-time matrix Q , corresponding to the eigenvalue of Eq. (3), contains dynamical information for constructing the outgoing electron flux. However, the derivation showing the connection between the wave function of the ejected electron and the eigenvector of the Q matrix is somewhat lengthy. We leave the detailed derivation in the Appendix, and single out only the main result in the following.

A time-dependent wave function describing a decaying system can be written as

$$\psi(\mathbf{r}, t) = \int_0^\infty \sum_j A_j^-(E) \Psi_{E_j}^-(\mathbf{r}) e^{-iEt} dE, \quad (4)$$

where $\Psi_{E_j}^-(\mathbf{r})$ is the time-independent wave function in the continuum, and atomic units are assumed. The coefficient $A_j^-(E)$ is the overlap between the continuum state $\Psi_{E_j}^-(\mathbf{r})$ and the resonant state $\Phi_R(\mathbf{r})$; $A_j^-(E) = \langle \Psi_{E_j}^-(\mathbf{r}) | \Phi_R(\mathbf{r}) \rangle$, which gives $\psi(\mathbf{r}, t) = \Phi_R(\mathbf{r})$ at $t=0$. Our task is to relate $A_j^-(E)$ to the eigenvectors of the Q matrix. This relation, derived in the Appendix, is

$$A_j^-(E) = \left(\frac{\Gamma}{2\pi} \right)^{1/2} \frac{1}{E - E_r + i\Gamma/2} W_j, \quad (5)$$

where W_j is the component of the normalized eigenvector of the Q matrix of channel j . The wave function $\Psi_{E_j}^-$ behaves asymptotically,

$$\Psi_{E_j}^-(\mathbf{r}) = \phi_j Y_{l_j 0} \exp[i(k_j r + \ln(2k_j r)/k_j - l_j \pi/2 + \sigma_{l_j})], \quad (6)$$

where ϕ_j is the core state wave function, k_j is the momentum, and σ_{l_j} is the Coulomb phase shift of channel j . There are incoming wave terms to the $\Psi_{E_j}^-(\mathbf{r})$ functions, but these terms do not contribute to Eq. (4) since at positive times the electron flux is completely directed outward. We are interested in angular distributions of ejected electrons that have

absorbed the same number of photons. The momentum k_j of the electrons is the same in the summation, and the terms which depend only on k_j contribute to an overall phase factor. For a fixed number of photons, the factor common to all channels is

$$F(E, r) = \left(\frac{\Gamma}{2\pi} \right)^{1/2} \frac{\exp\{i[kr + \ln(2kr)/k]\}}{E - E_R + i\Gamma/2}. \quad (7)$$

The time-dependent wave function is then

$$\psi(\mathbf{r}, t) = \int_0^\infty \sum_j W_j Y_{l_j 0} e^{i(\sigma_{l_j} - l_j \pi/2)} e^{-iEt} F(E, r) dE \quad (8)$$

if we restrict the summation to the channels in which the electrons have the same kinetic energy. The resonance width is assumed small and the angular factors and sum over j can be evaluated at the resonance energy before the integration is performed. The function in Eq. (8) separates into a radial function times an angular function, which can be identified with the angular distribution of the ejected electrons. Finally, the angular distribution is

$$\frac{d\sigma}{d\Omega} \propto \left| \sum_j W_j Y_{l_j 0} e^{i(\sigma_{l_j} - l_j \pi/2)} \right|^2, \quad (9)$$

since these are the only factors in Eq. (8) that depend on angle. The Q matrix is Hermitian, and its eigenvectors W_j are complex in general.

III. IONIZATION SPECTRA

Figure 1 shows the ionization rate as a function of laser frequency for the R matrix, the 3×3 Floquet calculations, and the experiment. The variation of the intensity of the laser with the frequency in the experiment has been taken into account in the calculations by making the intensity proportional to the dye gain curve. In presenting the figures, we have smoothed the experimental and theoretical curves a little to reduce the effect of the structured dye gain curve. The intensity in the calculation is about 6×10^{10} W/cm² at frequency $\omega = 14900$ cm⁻¹. It decreases as the frequency increases according to the dye gain curve in the experiment. In the 3×3 Floquet calculation, the dipole matrix elements $\mu_{2p,2s}$ and $\mu_{3d,2p}$ are evaluated in length form, and the wave functions are from the model potential eigenstates. Their values are $\mu_{2p,2s} = 0.751$ and $\mu_{3d,2p} = 0.642$, compared to the values 0.753 and 0.667 cited in Ref. [12]. There are significant differences between the R -matrix and the 3×3 Floquet calculations in the low frequency region.

The ionization rate in the 3×3 Floquet calculation was proportional to the intensity times the mixing coefficient of the $3d$ state. The R -matrix Floquet calculation, on the other hand, includes photon channels from $N = -2$ (two-photon emission) to $N = 5$ (five-photon absorption). This inclusion allows various combinations of emission and absorption in the ionization process. When the intensity reaches a certain value, the probability of emission may surpass absorption, and results in a decrease of ionization as the intensity increases [8]. The intensity in the calculation is for the edge of the laser beam, and represents the low intensity region. This

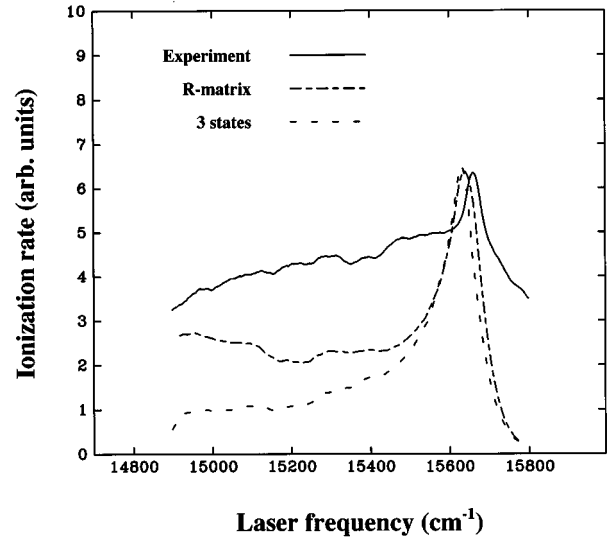


FIG. 1. Ionization spectrum as a function of laser frequency near the $3d$ state. The intensity in the calculation is 6×10^{10} W/cm² at $\omega = 14900$ cm⁻¹, and decreases toward the high-energy region according to the dye gain in the experiment. The width at the $3d$ state in the calculation is comparable to the experiment, but the magnitude is too small in the low-energy region.

intensity produces the right width of the $3d$ resonance, but the ionization rate is too small for frequencies away from the resonance. With twice the intensity (1.2×10^{11} W/cm² at frequency $\omega = 14900$ cm⁻¹) of Fig. 1, the ratio of the decay rate at the resonance to the decay rate away from the resonance can match the experiment, but the width of the $3d$ resonance is too broad (Fig. 2). This seems to support the scenario that the observed ionization spectrum is a mixture of ionization processes from different intensity regions in the laser. The width at the $3d$ resonance is mostly determined by the low intensity while, away from the resonance, the ioniza-

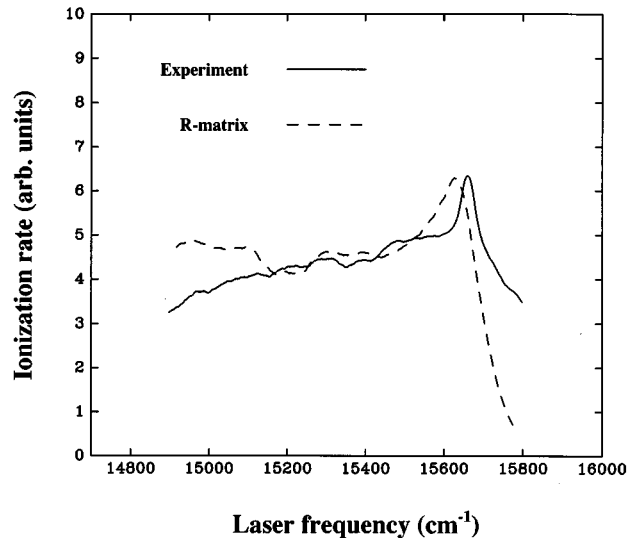


FIG. 2. Same as Fig. 1, but with twice the intensity in the calculation. The relative height between the resonant and the nonresonant regions is in agreement with the experiment, but the width at the $3d$ state is too large.

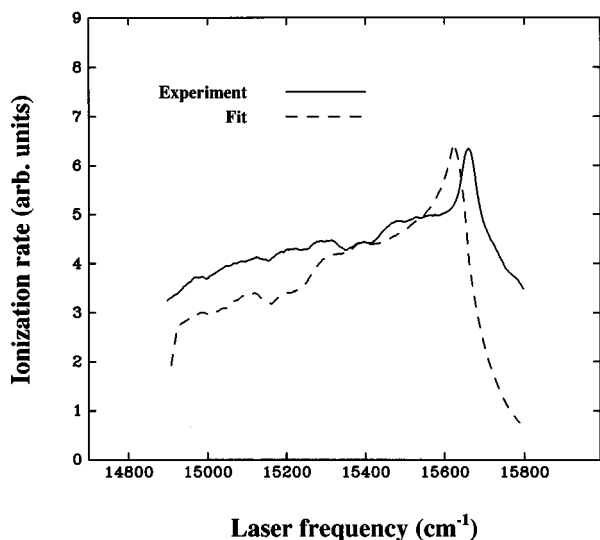


FIG. 3. Linear combinations of the 3×3 Floquet calculations with different intensities. This demonstrates a possible mechanism for quantitatively describing the ionization rates measured in the experiment.

tion is mainly from high intensity region.

The ionization probability of the ground state in a laser field depends on the intensity. Most importantly, the dependence on the intensity varies with the frequency. When the ground state is resonant with the $3d$ state, the ionization rate is linearly proportional to the intensity. In the nonresonant case, the dependence is the third power of the intensity if the interaction between the atom and the laser field is perturbative. At the intensity in the calculation, the dependence of the ionization rate with intensity in the R -matrix calculation shows we are not in the perturbation region. Away from the $3d$ resonance, the ionization is not proportional to the third power of intensity, as expected from the perturbation theory. The exact power depends on the energy of the ground Floquet state.

Moreover, the decay rate of the R -matrix calculation at $15\,000\text{ cm}^{-1}$ is greater than the decay rate at $15\,400\text{ cm}^{-1}$. Two factors contribute to this anomalous shape in the spectrum. First, the dye gain curve indicates that the intensity is decreasing from $\omega = 15\,000\text{ cm}^{-1}$ toward $\omega = 15\,400\text{ cm}^{-1}$. Second, at $\omega = 15\,000\text{ cm}^{-1}$, where $2p$ is 100 cm^{-1} away, the power of the dependence on the intensity is slightly lower than the power at $\omega = 15\,400\text{ cm}^{-1}$. The low intensity in the calculation suppresses the decay rate at $\omega = 15\,400\text{ cm}^{-1}$, more than $\omega = 15\,000\text{ cm}^{-1}$. The anomalous shape of the calculated spectrum will no longer occur if the calculation were performed using a higher intensity.

To demonstrate the possibility that the measured spectrum is a mixture of ionization processes from different intensity regions of the laser beam, we take the combination of several three-state Floquet calculations using different intensities, and the result is presented in Fig. 3. We choose intensities 3×10^{10} , 6×10^{10} , 1.2×10^{11} , 2.4×10^{11} , 4.8×10^{11} , and $9.6 \times 10^{11}\text{ W/cm}^2$, with mixing coefficients 26, 4, 4, 4, 1, and 1, respectively. Both the width and the relative heights agree with the experiment. The ionization measurement can thus be modeled as the multiphoton ionization of Li with a

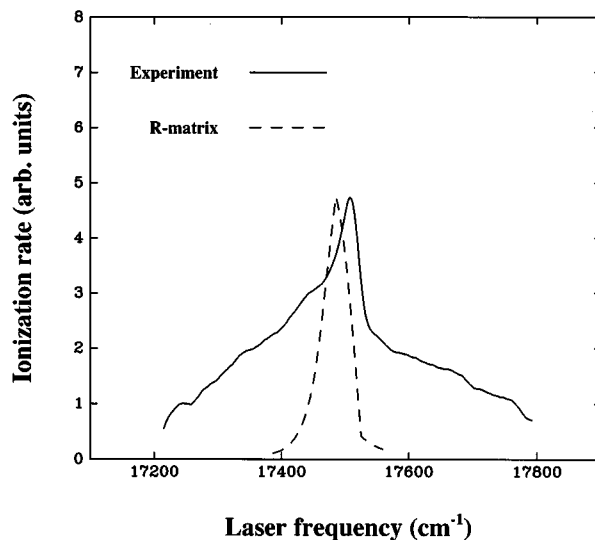


FIG. 4. Ionization spectrum near the $4s$ state at an intensity of $1.8 \times 10^{11}\text{ W/cm}^2$ at $17\,400\text{ cm}^{-1}$. The intensity at other frequencies were determined from the experimental dye gain curve. The calculated ionization rate decreases rapidly toward the nonresonant region.

distribution of laser intensities.

Figures 4 and 5 compare the experimental and theoretical ionization rates near the $4s$ and $4d$ resonance states respectively. The intensity of the calculation is $1.8 \times 10^{11}\text{ W/cm}^2$ at $17\,400\text{ cm}^{-1}$ for $4s$ resonance, and $2.0 \times 10^{11}\text{ W/cm}^2$ at $18\,000\text{ cm}^{-1}$ for $4d$ resonance. The two-photon absorption channels are treated as weakly closed in these calculations, unlike the calculations presented in Figs. 1–3. Again the ratio of the peak-to-background ionization rates in the calculation is larger than the experimental ratio. The calculation were performed for only one intensity curve; we thus expect the agreement between theory and experiment to be comparable to that shown in Fig. 1.

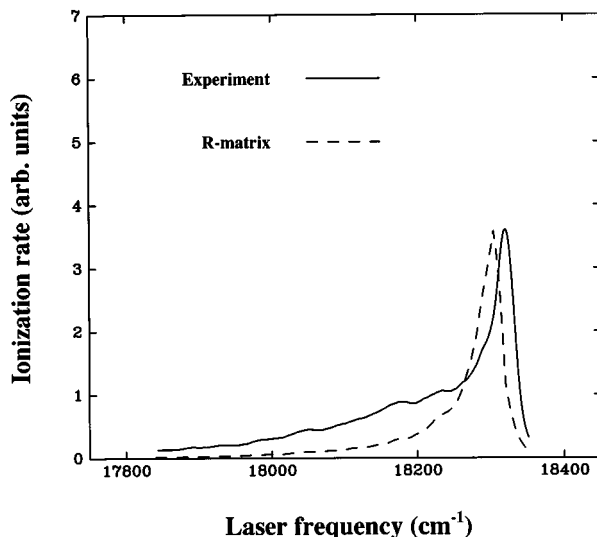


FIG. 5. Ionization spectrum near the $4d$ state for an intensity of $1.8 \times 10^{11}\text{ W/cm}^2$ at $18\,000\text{ cm}^{-1}$. The intensity at other frequencies were determined from the experimental dye gain curve.

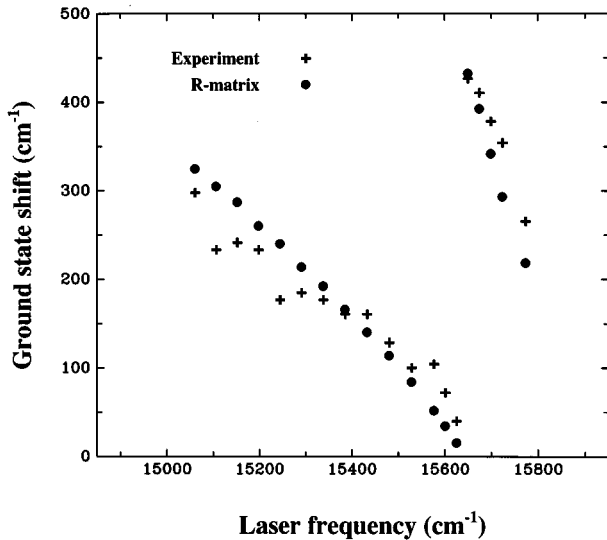


FIG. 6. Energy shift of the ground state near the $3d$ state for an intensity of 2×10^{11} W/cm 2 at $15\,060$ cm $^{-1}$. The intensity at other frequencies were determined from the experimental dye gain curve.

There is a puzzling discrepancy between the experimental and calculated ionization rates. The peak value of this rate is at a lower frequency in the calculation than in the experiment. The difference is larger than expected from experimental uncertainties in the wavelength, and from theoretical inaccuracies in the model potential. We have no good explanation for the discrepancy. The only semiplausible explanation is based on the breakdown of the adiabatic approximation when the photon is near resonance. When the frequency is near resonance, a Floquet state at low intensity may not evolve into *one* Floquet state at high intensity, but may evolve into a superposition of Floquet states. Near resonance, the experiment may be measuring the weighted decay rate of two states.

One of the interesting effects Li displays in a strong laser is the intensity dependence of the p and f wave branching ratios at different frequencies. Variations in the intensity can significantly change the branching ratio of the p wave, B_p , and f wave, B_f , in the calculation. When the ground Floquet state is below the $4s$ state ($E_{2s} + 2\hbar\omega < E_{4s}$), the increasing intensity will increase B_p/B_f . Thus the ground Floquet state acquires more $4s$ character than the $4d$. The situation is reversed if the frequency is increased so that the ground Floquet state is placed between the $4s$ and $4d$ states ($E_{4s} < E_{2s} + 2\hbar\omega < E_{4d}$). In that case, B_p/B_f decreases as the intensity increases.

A related issue to the ionization is the energy shift of the ground state. As all the quantum states evolve under the influence of the laser field, their relative positions may change as a result. This is known as the ac Stark shift. The energy shift of the ground state itself is not significant theoretically. But the shift of the ground state relative to other quantum states does provide a picture of how the electrons in the ground state may be ionized. The calculation shown in Fig. 6 is the energy shift of the ground state using the intensity profile in the experiment [20]. The calculation only uses the high intensity profile, and does not take into account the difference between the high and low intensity calculations.

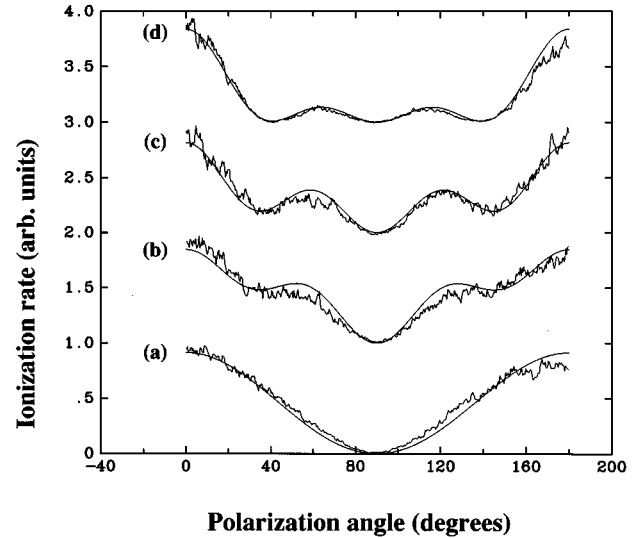


FIG. 7. Angular distribution of photoelectrons with intensity of 4.8×10^{11} W/cm 2 in the calculation. The frequencies were chosen so two photons were resonant or nearly resonant with the $4s$ and $4d$ states. The frequency varies so that the ground Floquet state is (a) resonant with the $4s$ state, (b) 25 cm $^{-1}$ above the $4s$ state, (c) 200 cm $^{-1}$ above the $4s$ state, or (d) 1554 cm $^{-1}$ above the $4s$ state. The pattern shows the electrons gain more and more f -wave character from (a) to (d). The branching ratios B_p/B_f are (a) 930, (b) 2.64, (c) 0.843, and (d) 0.055.

At frequencies between $15\,000$ and $15\,641$ cm $^{-1}$, a one-photon absorption would put the $2s$ state at a *higher* energy than the $2p$ state, which tends to shift the $2s$ state to higher energies, and a two-photon absorption would put the $2s$ state at a *lower* energy than the $3d$ state, which tends to shift the $2s$ state to lower energies ($E_{2p} - \hbar\omega < E_{2s} < E_{3d} - 2\hbar\omega$). The $2s$ - $2p$ coupling is the stronger coupling, and thus the $2s$ state is pushed to higher energy. However, as the frequency is increased, the $2s$ plus $2\hbar\omega$ state becomes more nearly degenerate with the $3d$ state, and $2s$ plus $\hbar\omega$ state becomes less degenerate with the $2p$ state; the upward shift in the Floquet energy thus decreases with the frequency. At frequencies above $15\,641$ cm $^{-1}$, $2s$ plus $2\hbar\omega$ state is above the $3d$ state; thus the interactions with the $2p$ and $3d$ states push the $2s$ state to higher energy. This accounts for the discontinuous jump in the shift at the frequency $15\,641$ cm $^{-1}$. As the frequency increases from $15\,641$ cm $^{-1}$, the energies become less degenerate, and therefore the shift decreases.

IV. ANGULAR DISTRIBUTION OF PHOTOELECTRONS

In Fig. 7, we plot the angular distribution of the electrons ejected from the Li atoms after absorbing three photons. In Fig. 7(a), the ground state is resonant with the $4s$ state after two photons are absorbed. The only ionization channel populated is the continuum p wave; the angular distribution is proportional to $\cos^2\theta$. In Fig. 7(d), the ground state is nearly resonant with the $4d$ state ($E_{2s} + 2\hbar\omega$ is 57 cm $^{-1}$ below the $4d$ state, where $\omega = 18\,283$ cm $^{-1}$). The $4d$ state can be ionized to p or f waves. The calculation shows that most of the photoelectrons are ejected as f waves. This is consistent with

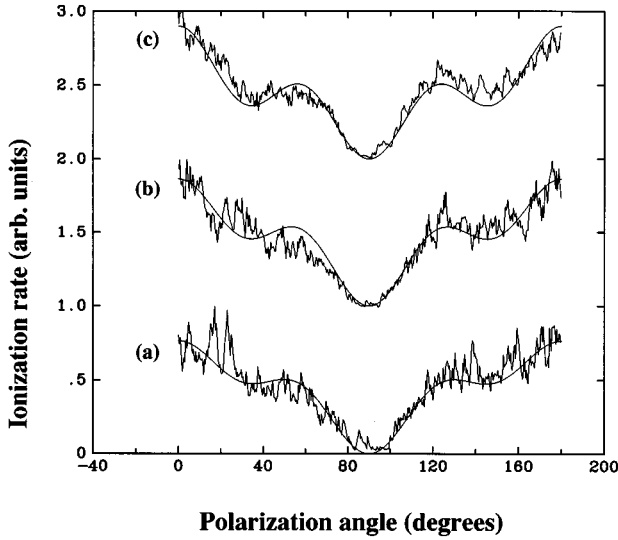


FIG. 8. Angular distribution of photoelectrons with the ground Floquet state 100 cm^{-1} above the $4s$ state ($E_{2s} + 2\hbar\omega = E_{4s} + 100 \text{ cm}^{-1}$). The intensity varies from (a) $0.5I$, (b) $0.7I$ to (c) I , with $I = 4.8 \times 10^{11} \text{ W/cm}^2$. The electrons gain f -wave character with higher intensity reflecting the nonlinear laser-atom interaction. The branching ratios B_p/B_f are (a) 3.17, (b) 2.27, and (c) 1.53.

the propensity rule [19], which states that the electron tends to gain angular momentum when it gains energy from the laser field.

The intensity chosen for these resonant calculations is not crucial. When the ground state is resonant with the $4s/4d$ state, it almost exclusively evolves to the resonant state ($4s/4d$) irrespective of the intensity. The angular symmetry of the resonant state determines into which channels the electron will go once it absorbs an additional photon. Because the resonant state is not strongly perturbed by the laser, the angular symmetry is uniquely determined by single-photon absorption from the resonant state. The probability of the electrons in the resonant state to be ionized is linearly proportional to the photon flux (the intensity). Hence the intensity only affects the ionization rate but not the angular distribution pattern. For Figs. 7(b) and 7(c), the photon frequency is such that two-photon absorption from the $2s$ state will be at an energy between the $4s$ and $4d$ states. In Fig. 7(b), the frequency is 17518.5 cm^{-1} , and for Fig. 7(c) the frequency is 17606 cm^{-1} . The relative amount of mixture between the ground state and the $4s$ and $4d$ states now depends on the intensity. The angular symmetry of the exit channels for the $4s$ and $4d$ states can interfere with each other. However, from the discussion in Sec. III, the measured distributions mainly arise from the high intensity part of the laser field. The intensity in the calculation ($4.8 \times 10^{11} \text{ W/cm}^2$) is close to the high intensity portion of the experiment, and it can represent most of the angular distribution measurement. A combination of multiintensity calculations may be needed to obtain a better agreement.

Figure 8 shows the calculations for various intensities with a frequency of 17556 cm^{-1} . The intensities are (a) $0.5I$, (b) $0.7I$ and (c) I , with $I = 4.8 \times 10^{11} \text{ W/cm}^2$. It can be seen from the figure that the relative amount of the f wave

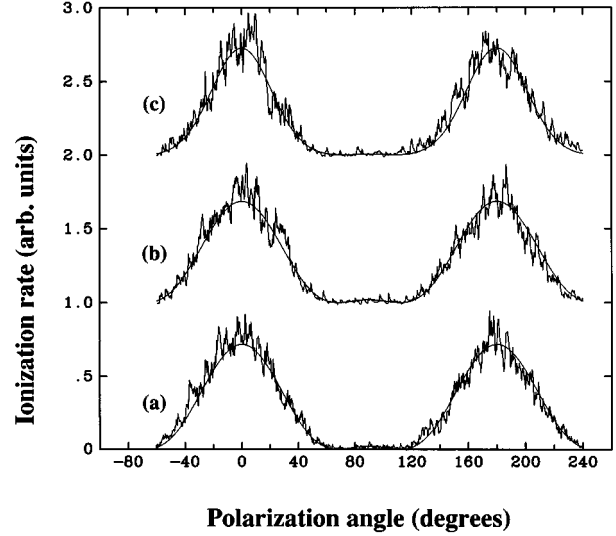


FIG. 9. Angular distribution of photoelectrons with four-photon absorption (the first above-threshold ionization) with intensity = $4.8 \times 10^{11} \text{ W/cm}^2$. The ground Floquet state is (a) 25 cm^{-1} below the $4s$ state, (b) resonant with the $4s$ state, and (c) 25 cm^{-1} above the $4s$ state. The pattern does not vary significantly as the frequency sweeps over the $4s$ state. The branching ratios B_s/B_d are (a) 0.423, (b) 0.424, and (c) 0.419.

increases as the intensity increases from (a) to (c). The ratio of the branching ratios of p to f waves, B_p/B_f decreases from 3.17 to 2.27 to 1.53 from (a) to (b) to (c). The ground state acquires more $4d$ character as the intensity increases, and the electrons are ionized to the f wave. This is a manifestation of the nonlinear laser-atom interaction. For a fixed laser frequency, the ratio B_p/B_f should not change with the laser intensity to lowest-order in perturbation theory. This can be seen by calculating the mixing coefficients using perturbation theory. In lowest-order perturbation theory the admixture of $4s$ and $4d$ states into the $2s$ ground state is

$$A_{4s} = I \frac{\langle 2s|z|2p\rangle\langle 2p|z|4s\rangle}{(E_{2s} + \hbar\omega - E_{2p})(E_{2s} + 2\hbar\omega - E_{4s})} \quad (10)$$

for the $4s$ state, and

$$A_{4d} = I \frac{\langle 2s|z|2p\rangle\langle 2p|z|4d\rangle}{(E_{2s} + \hbar\omega - E_{2p})(E_{2s} + 2\hbar\omega - E_{4d})} \quad (11)$$

for the $4d$ state, where I is the intensity of the laser field. Both of the states mix with the ground state at second order in perturbation theory (reflecting two-photon absorption), and therefore both of the mixing coefficients are proportional to the laser intensity. The ratio of the amplitudes, and therefore the ratios of the probabilities, is independent of the laser intensity of this order.

Figure 9 is the experimental and calculated angular distributions for the above-threshold ionization (ATI) with four-photon absorption. The angular distribution pattern does not change over the total 25-cm^{-1} variation in the frequency. In lowest-order perturbation theory, the electrons can be ejected as s , d , or g waves after absorbing four photons. The calculation shows that the branching ratio for the continuum d

wave to the s wave is 2.4, and that this does not vary significantly as the frequency varies over the $4s$ resonance; the probability of ejection as g waves is very small. A simple application of the propensity rules would suggest the g waves should have the highest probability of ejection. This propensity is suppressed because the g waves do not have a large enough energy to penetrate the angular momentum barrier and reach the ionization region. An interesting aspect of the ATI angular distribution is that the ratio of the s and d coefficients in Eq. (9) is nearly real. This was not true of the three-photon angular distributions; the ratio of the p to f coefficients in Eq. (9) was complex. In comparing Figs. 7 and 8 with Fig. 9, it is clear that the angular distribution for the ATI electrons is more strongly peaked along the direction of laser polarization than the angular distribution for three-photon absorption. This behavior arises from the fact that the laser can only do work on the electron in the polarization direction. The propensity rule is that as more photons are absorbed the angular distribution becomes more strongly peaked.

V. CONCLUSION

In summary, we have applied the mixed gauge R -matrix Floquet method to calculate the ionization rate and angular distribution of electrons ejected from Li in a laser field. The angular distribution calculations are in good agreement with the experiment. The intensity of the laser used in the calculation of the angular distribution indicates that the photoelectrons come mainly from the high intensity part of the laser beam. The calculations of the ionization rate as a function of laser frequency suggest that the measured spectrum is a mixture of ionization processes from the intensity distribution in the laser beam. A superposition of calculations with various intensities is necessary to obtain the agreement with the experiment. Overall, the R -matrix Floquet method is useful to understand multiphoton processes in atoms, and to reproduce experimental measurements quantitatively.

ACKNOWLEDGMENTS

We thank Dr. T. F. Gallagher and Dr. D. I. Duncan for providing us with the experimental data necessary for our calculations. We also thank Dr. D. I. Duncan for a detailed explanation of the experimental conditions. This work was partly supported by a grant from Auburn University and by a NSF Young Investigator Grant No. PHY9457903.

APPENDIX

This Appendix gives a detailed derivation of the coefficient A_j^- in Eq. (4), which leads to the angular distribution in Eq. (9). The purpose of this derivation is to show that A_j^- is simply proportional to the eigenvectors of the delay-time matrix Q . We start with the exact solutions of the Schrödinger equation $(E-H)F_\alpha=0$ for the continuum states, assuming no coupling to the closed channels. The regular solution outside the short-range interaction region is

$$F_\alpha = \sum_i \phi_i (f_i \cos \pi \mu_\alpha - g_i \sin \pi \mu_\alpha) U_{i\alpha}, \quad (\text{A1})$$

where ϕ_i is the core-state wave function, f_i and g_i are the regular and irregular Coulomb wave functions, μ_α is the eigen quantum defect, and U is the rotation matrix needed to construct the eigenchannel α . Similarly, the corresponding irregular solution outside the short-range interaction region is

$$G_\alpha = \sum_i \phi_i (f_i \sin \pi \mu_\alpha + g_i \cos \pi \mu_\alpha) U_{i\alpha}. \quad (\text{A2})$$

For the case we are interested in in this paper, the widths of the resonant states are relatively small. It suffices to consider a well-isolated resonance state which has an energy E_R ,

$$\langle \Phi_R | H | \Phi_R \rangle = E_R, \quad (\text{A3})$$

where Φ_R is the wave function of the resonance state. Now, consider the coupling between the continuum and the resonance state. Because the existence of the resonant state, the continuum state becomes

$$\psi_\alpha = \sum_{\alpha'} (F_{\alpha'} \delta_{\alpha'\alpha} - G_{\alpha'} \bar{K}_{\alpha'\alpha}). \quad (\text{A4})$$

From the Kohn variational principle, we approximate the matrix $\bar{K}_{\alpha'\alpha}$ by

$$\bar{K}_{\alpha'\alpha} = -\pi \langle \psi'_{\alpha'} | H - E | \psi'_{\alpha'} \rangle, \quad (\text{A5})$$

where the trial wave function $\psi'_{\alpha'} = F_{\alpha'} + \Phi_R A_{\alpha'}$. Φ_R is orthogonal to $F_{\alpha'}$, which means that $A_{\alpha'} = \langle \psi'_{\alpha'} | \Phi_R \rangle$. By variation with respect to $A_{\alpha'}$, we find

$$A_{\alpha'} = \frac{\langle F_{\alpha'} | V | \Phi_R \rangle}{E - E_R} \equiv \frac{V_{\alpha'R}}{\sqrt{\pi}(E - E_R)} \quad (\text{A6})$$

where $V_{\alpha'R} = \sqrt{\pi} \langle F_{\alpha'} | V | \Phi_R \rangle$ and

$$\bar{K}_{\alpha'\alpha} = -\frac{V_{\alpha'R}(V^T)_{R\alpha}}{E - E_R}. \quad (\text{A7})$$

In matrix form,

$$\bar{\mathbf{K}} = -\frac{\mathbf{V} \cdot \mathbf{V}^T}{E - E_R}, \quad (\text{A8})$$

and the width of the resonance Γ is related to \mathbf{V} by

$$\mathbf{V}^T \mathbf{V} = \Gamma/2, \quad (\text{A9})$$

where Γ is assumed to be small. We can also construct the $\bar{\mathbf{S}}$ matrix in terms of \mathbf{V} ,

$$\bar{\mathbf{S}} = \frac{1+i\bar{\mathbf{K}}}{1-i\bar{\mathbf{K}}} = \mathbf{1} - i2\mathbf{V} \left(\frac{1}{E - E_R + i\Gamma/2} \right) \mathbf{V}^T. \quad (\text{A10})$$

The eigenchannel wave functions that satisfy the outgoing (incoming) wave boundary condition are obtained through

$$\psi^\pm = \psi \frac{1}{1 \pm i\bar{\mathbf{K}}}. \quad (\text{A11})$$

The coefficient A_α is transformed accordingly:

$$\mathbf{A}^\pm = \frac{1}{\mathbf{1} \pm i\mathbf{K}} \mathbf{A} = \frac{\mathbf{V}}{\sqrt{\pi}} \frac{1}{E - E_R \mp i\Gamma/2}. \quad (\text{A12})$$

Up to this moment, all the formulations are expressed using the eigenchannel wave function ψ_α . To express the coefficients A in terms of ψ_j , we note that

$$\sum_\alpha (-G_\alpha \pm iF_\alpha) e^{\mp i\pi\mu_\alpha} U_{\alpha j}^\dagger = \phi_j(-g_j \pm if_j). \quad (\text{A13})$$

The wave functions and the coefficients are then

$$\psi_j^\pm = \sum_\alpha \psi_\alpha^\pm e^{\pm i\pi\mu_\alpha} U_{\alpha j}^\dagger \quad (\text{A14})$$

and

$$A_j^\pm = \sum_\alpha U_{j\alpha} e^{\mp i\pi\mu_\alpha} \frac{V_{\alpha R}}{\sqrt{\pi}} \frac{1}{E - E_R \mp i\Gamma/2}. \quad (\text{A15})$$

The expression for A_j^- in Eq. (A15) can be calculated based on the information we had. However we are going to show that this expression can be further simplified and related to the eigenvectors of the delay-time matrix. This reduces the effort to obtain the angular distribution of the ejected electrons.

With the basis function ψ_j , the scattering matrix \mathbf{S} and the delay-time matrix \mathbf{Q} are

$$S_{jk} = \sum_{\alpha\alpha'} U_{j\alpha} e^{i\pi\mu_\alpha} \bar{S}_{\alpha\alpha'} e^{-i\pi\mu_{\alpha'}} U_{\alpha'k}^\dagger \quad (\text{A16})$$

and

$$Q_{jk} = \sum_{\alpha\alpha'} U_{j\alpha} e^{i\pi\mu_\alpha} \bar{Q}_{\alpha\alpha'} e^{-i\pi\mu_{\alpha'}} U_{\alpha'k}^\dagger. \quad (\text{A17})$$

The eigenvector of matrix \mathbf{Q} , W_j , and the eigenvector of matrix $\bar{\mathbf{Q}}$, \bar{W}_j , can be related through

$$\sum_k Q_{jk} W_k = q W_j \quad (\text{A18})$$

and

$$\sum_{\alpha'} \bar{Q}_{\alpha\alpha'} \bar{W}_{\alpha'} = q \bar{W}_\alpha. \quad (\text{A19})$$

From Eq. (A17), we have

$$W_j = \sum_\alpha U_{j\alpha} e^{i\pi\mu_\alpha} \bar{W}_\alpha. \quad (\text{A20})$$

To obtain \bar{W}_α , we note

$$\bar{\mathbf{Q}} = -i \frac{d\bar{\mathbf{S}}}{dE} \bar{\mathbf{S}}^\dagger \quad (\text{A21})$$

and using Eqs. (A9) and (A10), we obtain

$$\bar{\mathbf{Q}} = \mathbf{V} \frac{2}{(E - E_R)^2 + (\Gamma/2)^2} \mathbf{V}^T. \quad (\text{A22})$$

The relation between the eigenvalue q and the width of the resonance is governed by Eq. (3), and we should have

$$\bar{\mathbf{Q}} \cdot \bar{\mathbf{W}} = \bar{\mathbf{W}} \frac{\Gamma}{(E - E_R)^2 + (\Gamma/2)^2}. \quad (\text{A23})$$

Equation (A22) then implies

$$\bar{W}_\alpha = \left(\frac{2}{\Gamma}\right)^{1/2} V_{\alpha R}. \quad (\text{A24})$$

Finally, from Eq. (A20),

$$W_j = \sum_\alpha U_{j\alpha} e^{i\pi\mu_\alpha} \left(\frac{2}{\Gamma}\right)^{1/2} V_{\alpha R}, \quad (\text{A25})$$

and, put in matrix form and using Eq. (A12),

$$\begin{aligned} \mathbf{W} &= \mathbf{U} e^{i\pi\mu_\alpha} \left(\frac{2}{\Gamma}\right) \mathbf{V} \\ &= \left(\frac{2\pi}{\Gamma}\right)^{1/2} (E - E_R + i\Gamma/2) \mathbf{A}^-. \end{aligned} \quad (\text{A26})$$

Inverting the matrix equation, we find the coefficient

$$A_j^- = \left(\frac{\Gamma}{2\pi}\right)^{1/2} \frac{1}{E - E_R + i\Gamma/2} W_j. \quad (\text{A27})$$

A_j^- is the coefficient in Eq. (5), and it serves to demonstrate that the energy distribution of the wave function is proportional to the eigenvector of the delay-time matrix. Thus the delay-time matrix Q is useful in multiphoton ionization problems, for which its largest eigenvalue is related to ionization rate, and its eigenvectors are connected to angular distributions of the ejected electrons.

-
- [1] S. I. Chu and J. Cooper, Phys. Rev. A **32**, 2769 (1985).
 [2] R. M. Potvliege and R. Shakeshaft, Phys. Rev. A **40**, 3061 (1989).
 [3] L. A. Collins and G. Csanak, Phys. Rev. A **44**, R5343 (1991).
 [4] J. L. Krause, K. J. Schafer, and K. C. Kulander, Phys. Rev. A **45**, 4998 (1992).

- [5] H. Xu, X. Tang, and P. Lambropoulos, Phys. Rev. A **46**, R2225 (1992).
 [6] P. G. Burke, P. Francken, and C. J. Joachain, Europhys. Lett. **13**, 617 (1990).
 [7] P. G. Burke, P. Francken, and C. J. Joachain, J. Phys. B **24**, 761 (1991).

- [8] M. Dörr, P. G. Burke, C. J. Joachain, C. J. Noble, J. Purvis, and M. Terao-Dunseath, *J. Phys. B* **26**, L275 (1993).
- [9] R. Grobe and J. H. Eberly, *Phys. Rev. A* **48**, 4664 (1993).
- [10] L. Dimou and F. H. M. Faisal, *J. Phys. B* **27**, L333 (1994).
- [11] M. Dörr, C. J. Joachain, R. M. Potvliege, and S. Vucic, *Phys. Rev. A* **49**, 4852 (1994).
- [12] D. I. Duncan, J. G. Story, and T. F. Gallagher, *Phys. Rev. A* **52**, 2209 (1995).
- [13] H. G. Muller and H. B. van Linden van den Heuvell, *Laser Phys.* **3**, 694 (1993).
- [14] F. Robicheaux, C.-T. Chen, P. Gavras, and M. S. Pindzola, *J. Phys. B* **28**, 3047 (1995).
- [15] H. Rottke, B. Wolff-Rottke, D. Feldmann, K. H. Welge, M. Dörr, R. M. Potvliege, and R. Shakeshaft, *Phys. Rev. A* **49**, 4837 (1994).
- [16] F. T. Smith, *Phys. Rev.* **118**, 349 (1960).
- [17] C. E. Moore, in *Atomic Energy Levels*, edited by C. E. Moore, Natl. Bur. Stand. (U.S.) No. 35 (U.S. GPO, Washington, DC, 1971), Vol. 1.
- [18] W. Johnson, D. Kohb, and K.-N. Huang, *At. Data Nucl. Data Tables* **28**, 333 (1983).
- [19] U. Fano, *Phys. Rev. A* **32**, B617 (1985).
- [20] D. I. Duncan (private communication).